Geometrical Correction for the Inter- and Intramolecular Basis Set Superposition Error in Periodic Density Functional Theory Calculations

J.G. Brandenburg, M. Alessio, B. Civalleri, M. F. Peintinger, T. Bredow, S. Grimme
A geometrical correction for the inter- and intra-molecular basis set superposition error in periodic density functional theory calculations.
Journal of Physical Chemistry A, 117, 9282-9292, 2012, DOI: 10.1021/jp406658y.

A Geometrical Correction for the Inter- and Intra-Molecular Basis Set Superposition Error in Periodic Density Functional Theory Calculations

Jan Gerit Brandenburg,[†] Maristella Alessio,[‡,¶] Bartolomeo Civalleri,[‡] Michael F. Peintinger,[†] Thomas Bredow,[†] and Stefan Grimme[*,†]

Mulliken Center for Theoretical Chemistry, Institut für Physikalische und Theoretische Chemie der Universität Bonn, Beringstraße 4, 53115 Bonn, Germany, and Department of Chemistry and Centre of Excellence NIS, University of Turin, Via P. Giuria 7, 10125 Torino, Italy

E-mail: grimme@thch.uni-bonn.de

[*]To whom correspondence should be addressed

[†]Mulliken Center for Theoretical Chemistry, Institut für Physikalische und Theoretische Chemie der Universität Bonn, Beringstraße 4, 53115 Bonn, Germany

[‡]Department of Chemistry and Centre of Excellence NIS, University of Turin, Via P. Giuria 7, 10125 Torino, Italy

[¶]Present address: Department of Chemistry, Humboldt University, Berlin, Germany

Abstract

We extend the previously developed geometrical correction for the inter- and intra-molecular basis set superposition error (gCP) to periodic Density Functional Theory (DFT) calculations. We report gCP results compared to those from the standard Boys-Bernardi counterpoise correction scheme and large basis set calculations. The applicability of the method to molecular crystals as the main target is tested for the benchmark set X23. It consists of 23 non-covalently bound crystals as introduced by Johnson *et. al.* (*J. Chem. Phys.* **2012**, *137*, 054103) and refined by Tkatchenko *et. al* (*J. Phys. Chem. Lett.* **2013**, *4*, 1028). In order to accurately describe long-range electron correlation effects, we use the standard atom-pairwise dispersion correction scheme DFT-D3. We show that a combination of DFT energies with small atom-centered basis sets, the D3 dispersion correction, and the gCP correction can accurately describe van der Waals and hydrogen bonded crystals. Mean absolute deviations of the X23 sublimation energies can be reduced by more than 70% and 80% for the standard functionals PBE and B3LYP, respectively, to small residual mean absolute deviations of about 2 kcal/mol (corresponding to 13 % of the average sublimation energy). As a further test we compute the interlayer interaction of graphite for varying distances and obtain good equilibrium distance and interaction energy of 6.75 Å and -43.0 meV/atom at the PBE-D3-gCP/SVP level. We fit the gCP scheme for a recently developed pob-TZVP solid-state basis set and obtain reasonable results for the X23 benchmark set and the potential energy curve for water adsorption on a nickel (110) surface.

Introduction

The theoretical description of periodic systems using Density Functional Theory (DFT) or Hartree-Fock (HF) with moderate computational costs is highly desirable. Especially the computation of reliable sublimation energies, geometries and relative energies of molecular crystals and their polymorphic forms is of utmost importance, i.e., aiming at crystal structure prediction.[1–3] The theoretical evaluation of molecular crystals and their polymorphs is an active research field.[4–10]

Bulk metals have a strongly delocalized valence electron density and therefore, originless plane-wave based basis sets are probably the best choice in orbital based methods.[11] In molecular crystals, on the other hand, the charge density is more localized. Thus, for plane-wave based methods huge basis sets are needed. We have recently found that for a typical system of stacked organic π-systems, up to $1.5 \cdot 10^5$ projector augmented plane-wave (PAW) basis functions must be considered for accurate results.[12] For this and similar systems, atom-centered basis functions could be much more efficient.[13–16]

Small atom-centered basis sets strongly suffer from basis set errors (BSE), especially the basis set superposition error (BSSE). For molecular systems, a number of different correction schemes exist. The Ref.[17] gives a good review of the various approaches. Recently, we have mapped the standard Boys-Bernardi counterpoise correction (BB-CP) onto a semi-empirical atom-pairwise potential.[18] This repulsive potential was fitted for a number of typical basis sets and depends only on the system geometry and was therefore denoted as geometrical counterpoise correction (gCP). Analytic gradients are problematic in nearly all other counterpoise schemes, but are easily and efficiently obtained within the gCP. Moreover, the accidental error cancellation in standard small basis set calculations was recently demonstrated for molecular thermochemistry and results could be significantly improved by applying gCP.[19]

In this work we include periodic boundary conditions and unit cell gradients in the gCP code. We correct the (semi) local density functionals for missing long-range electron correlation, also known as van der Waals or London dispersion interaction, with the DFT-D3 method.[20] The theory of both correction schemes, D3 and gCP, is briefly discussed. The proposed approach could also be applied analogously to HF calculations but we restrict ourselves to DFT in this work. Computational details are summarized and a short comparison of gCP and BB-CP energies is given. We test the applicability of the DFT-D3-gCP (or 'functional'-D3-gCP) denoted method on the X23 benchmark set[21,22] for non-covalent interactions in molecular crystals and for the interaction between graphite layers. Furthermore, gCP parameters are calculated for a new solid-state optimized basis (pob-TZVP) and tested on the X23 sublimation energies, the graphite stacking, and for water

adsorption on a nickel (110) surface. Finally, we give a conclusion.

Theory

We split the BSE into basis set incompleteness error (BSIE) and BSSE. The BSIE arises always, when finite incomplete basis sets are used. The BSSE is due to an inhomogeneous basis, i.e., the variational freedom varies in different spacial regions. In the description of periodic systems, two types of single particle basis sets are the most prominent, (1) a superposition of orthonormal plane-waves spread uniformly in space which is BSSE-free and (2) a direct product of a superposition of atom-centered functions and a momentum ($\mathbf{k}$) dependent phase factor enforcing the correct translational symmetry. The atom-centered orbitals are typically contracted from primitive Gaussian functions with different exponents to decrease the computational effort. In the dissociation limit, each atom can be accurately described by this set. It is possible to choose the 'most important' atom-centered basis functions and to minimize the BSIE with a fixed number of basis functions. Moreover, the use of Gaussian basis sets presents some advantages: core electrons can be easily treated, the algorithms are similar to those used in efficient molecular quantum chemistry codes where Gaussian orbitals are generally adopted, and the quasi-local character of electronic structure (at least for insulators) is more naturally exploited. However, incomplete, atom-centered basis sets always favor certain spatial locations.

Two major manifestations of the BSSE arise: (1) In the calculation of cohesive energies the presence of surrounding molecules increases the basis relative to that in the dissociation limit leading to an artificial overbinding; (2) In geometry optimizations the atomic centers move and therefore the basis changes, too. Unit cell volumes are artificially underestimated. A complete basis set is BSE-free, so the best way to avoid both BSIE and BSSE, is to increase the basis set and this is always recommended if technically possible.

Unfortunately, in most periodic systems large atom-centered basis sets are not commonly affordable. This is particularly relevant when diffuse functions with small Gaussian exponents are

included. While they are important to describe the tails of molecular density distributions, they are less needed in periodic systems because the overlap between Bloch functions is higher than between AOs in finite systems. Diffuse functions may lead to quasi-linear basis set dependencies which can cause an instability in the convergence of the iterative solution of the Kohn-Sham or HF equations (SCF procedure). Practically, it turns out to be difficult to enlarge the basis to the quadruple-ζ level, even in not very dense solids, although polarized triple- and quadruple-ζ basis sets have been employed occasionally in calculations on molecular crystals.[6,23–25] Recently, a consistent triple-ζ basis set for periodic systems was developed by some of us, which aims to overcome some of the mentioned problems.[26] Therein, basis functions with very small exponents are consistently replaced by more localized contracted orbitals. However, we show below that the BSSE of this basis is still very large for typical cases and must be corrected.

Another problem of HF and common (semi-local) DFT functionals is that they are not capable of describing long-range electron correlation, a.k.a. London Dispersion interaction. In order to get physically reasonable results, the methods have to be properly dispersion corrected.[27] We decompose the total energy E_{tot} of a system into DFT/HF energy $E_{\text{DFT/HF}}$, dispersion energy E_{disp}, and additional counterpoise correction E_{gCP}:

$$E_{\text{tot}} = E_{\text{DFT/HF}} + E_{\text{disp}} + E_{\text{gCP}}\,. \tag{1}$$

To accurately describe the London dispersion interaction, we use our latest semi-classical *ab-initio* dispersion correction DFT-D3.[20,28] It incorporates non-empirical, pairwise-specific, chemical environment-dependent dispersion coefficients, a physically sound damping function according to Becke and Johnson,[29] and optionally a non-additive Axilrod-Teller-Muto three-body dispersion term.[30] The dispersion energy can be split into two- and three-body contributions $E_{\text{disp}} =$

$E^{(2)} + E^{(3)}$:

$$E^{(2)} = -\frac{1}{2} \sum_{n=6,8} \sum_{A \neq B}^{\text{atom pairs}} \sum_{\mathbf{T}} s_n \frac{C_n^{AB}}{\|\mathbf{r}_B - \mathbf{r}_A + \mathbf{T}\|^n + f(R_0^{AB})^n} \tag{2}$$

$$E^{(3)} = -\frac{1}{6} \sum_{A \neq B \neq C}^{\text{atom triples}} \sum_{\mathbf{T}} \frac{C_9^{ABC} \, (3\cos\theta_a \cos\theta_b \cos\theta_c + 1)}{{r_{ABC}}^9 \cdot (1 + 6(r_{ABC}/R_0)^{-\alpha})} \,. \tag{3}$$

Here, C_n^{AB} denotes the averaged (isotropic) n^{th}-order dispersion coefficient for atom pair AB, and $\mathbf{r}_{A/B}$ are their Cartesian positions. The real-space summation over all unit cells is done by considering all translation invariant vectors $\mathbf{T}$ inside a cut-off sphere. The scaling parameter s_6 equals unity for the here applied functionals and ensures the correct limit for large distances, and s_8 is a functional-dependent scaling factor. The rational damping function $f(R_0^{ab})$ is

$$f(R_0^{ab}) = a_1 R_0^{ab} + a_2 \,, \; R_0^{ab} = \sqrt{\frac{C_8^{ab}}{C_6^{ab}}} \,. \tag{4}$$

The dispersion coefficients are obtained from first-principle calculations for molecular systems with time-dependent DFT and and application of the Casimir-Polder relation.[31] The three parameters s_8, a_1, and a_2 are fitted for each functional (or HF) on a benchmark set of small, non-covalently bound molecules. The fitting is necessary to prevent double counting of dispersion interactions at short range and to adjust repulsive and attractive parts. This procedure has an impact on the short- to medium-ranged part of the dispersion energy, but does not affect the long-range regime, which is most important for periodic systems. In the three-body contribution, r_{ABC} corresponds to an averaged distance between the three pairs and $\theta_{a/b/c}$ are the corresponding angles. The general applicability of this atom-pairwise dispersion correction was shown in a number of recent publications by us[32–34] and other groups[8,35,36] and also for solids.[12,37–40] The importance of three- and many-body dispersion effects is currently not clear but this question is intensively investigated.[34,41,42]

The most frequently used method to correct for the BSSE is the Boys-Bernardi counterpoise

(BB-CP)[43] method. For a dimer AB with basis functions a and b, respectively, it reads

$$E_{\text{BB-CP}} = \{E(\text{A})_a - E(\text{A})_{ab}\} + \{E(\text{B})_b - E(\text{B})_{ab}\} \,, \tag{5}$$

where $E(A)_a$ is the energy of fragment A with basis functions a and $E(A)_{ab}$ denotes the energy of the same fragment A with the enlarged basis ab. In the geometric counterpoise correction scheme, we map the BB-CP onto a semi-empirical, repulsive pair potential $V_A(r)$, which decays exponentially with the inter-atomic distance r:

$$V_A(r) = e_A^{\text{miss}} \frac{\exp\left(-\alpha \cdot r^{\beta}\right)}{\sqrt{S \cdot N_B^{\text{virt}}}} \,. \tag{6}$$

The energy difference between a large and the generally smaller target basis set for an atom A inside a weak electric field e_A^{miss} is computed for all atoms. This quantity measures the incompleteness of the atomic target basis. The potential is normalized by the Slater-overlap S, the number of virtual orbitals $N_{\text{B}}^{\text{virt}}$, and the empirical parameters α and β. The Slater exponents of s- and p-valence orbitals ζ_s and ζ_p, respectively, are averaged to get a single s-function exponent ζ_s^*

$$\zeta_s^* = \eta \, \frac{\zeta_s + \zeta_p}{2} \,, \tag{7}$$

with fit parameter η. In order to satisfy the periodic boundary conditions (PBC), the summation runs over all distinct pairs AB inside a large super-cell of certain radius. Using a real-space cut-off is possible because of the exponential decay, which converges rapidly with increasing distance. We sum over all atom pairs and get the energy E_{gCP}:

$$E_{\text{gCP}} = \frac{\sigma}{2} \sum_{A \neq B}^{\text{atom pairs}} \sum_{\mathbf{T}} V_A(\|\mathbf{r_A} - \mathbf{r_B} + \mathbf{T}\|) \,, \tag{8}$$

with a global scaling parameter σ.

Altogether, gCP involves four fit parameters (σ, α, β, η) for each basis set. They have been

fitted to reproduce the BB-CP energy of the large S66 $\times$ 8 non-covalent interaction benchmark set[44] by minimizing the root-mean-square deviation. No parameter re-fit is considered here nor needed here for the applied standard basis sets (the new pob-TZVP basis[26] is discussed separately) because a short-range potential should not be affected by PBC. Parameters are available for a variety of basis sets, namely the Ahlrichs-type basis sets SV, def2-SVP, and def2-TZVP,[45–47] the minimal basis set MINIS,[48,49] and the Pople-style basis 6-31G*.[50]

Computational Details

We calculate the HF and DFT energies mostly with the widely used crystalline-orbital program CRYSTAL09.[51,52] In the CRYSTAL code, the Bloch functions are obtained by a direct product of a superposition of atom-centered Gaussian functions and a **k** dependent phase factor. We use the generalize gradient approximated (GGA) functional PBE[53,54] and the hybrid GGA functional B3LYP.[55,56] The Γ-centered **k**-point grid is generated via the Monkhorst-Pack scheme[57] with one **k**-point for molecular calculations, four **k**-points for molecular crystals, and 12**k**-points in each direction for graphite. The large integration grid (LGRID) and tight tolerances for Coulomb and exchange sums are used. The self consistent field (SCF) energy threshold is set to 10^{-8} Hartree. We exploit the polarized and unpolarized split-valence basis set SVP and SV and the triple-ζ basis set pob-TZVP. Calculations close to the complete basis set limit (CBS) are carried out with the Vienna Ab-initio Simulation Package VASP 5.3.[58,59] We utilize the GGA functional PBE in combination with a projector-augmented plane wave basis set (PAW)[60,61] with a huge energy cut-off of 1000 eV. This corresponds to $\sim$ 200% of the recommended high-precision cut-off and should accurately approximate the CBS for the here investigated properties (denoted as PBE/CBS in the following).

We include the dispersion energy with the *dftd3* program in the Becke-Johnson damping scheme and a conservative distance cut-off radius of 95 Bohr. The BSSE correction is added via the gCP method as discussed above where a smaller cut-off radius of 60 Bohr is used. Compared to the

computation of the HF or DFT energies and gradients, the dispersion and counterpoise contributions requires practically no additional computation time (even in a small basis, the HF or DFT calculation is one to two orders of magnitudes slower).

The gCP correction will be also compared with the BB-CP scheme. In CRYSTAL, the BB-CP method is applied by supplementing the basis set of a single molecule, as cut out from the crystal structure, with the functions of an increasing number of atoms (ghost atoms) belonging to the surrounding array of molecules within a sphere of a given radius. Here, a sphere of 4.0 Å from each atom of the molecule was used. Tests with a larger radius of the sphere show a change of the lattice energies by only a few tenths of a kcal/mol.

For the geometry optimization, we use an extended version of the approximate normal coordinate rational function optimization program (ANCOPT).[62] The Cartesian coordinates of all atoms in one unit cell are transformed into approximate normal coordinates. In order to obtain reasonable internal coordinates, we translate all atoms by multiples of unit cell vectors in such a way that all molecular fragments are directly connected. We use a rational function algorithm to calculate the new coordinates from analytic atomic gradients and an interpolated Hessian matrix of second derivatives.[63]

Common unit cell optimizer rescale all atom positions inside the unit cell to get the new coordinates. For molecular crystals, this procedure is very inefficient because all intramolecular distances change and therefore all atom gradients rise significantly. We perform a slightly different cell step. We identify all molecular fragments, calculate their center of mass, and transform all these centers according to the new cell matrix. This keeps the intramolecular distances fixed and we need less optimization steps. Full convergence is achieved if the energy change is below 10^{-6} Hartree and if the gradient thresholds for the total atomic gradient (10^{-4} Hartree/Bohr) and total cell gradient (10^{-3} Hartree/Bohr) are fulfilled.

Comparison of Counterpoise Corrections

We first compare the gCP and BB-CP correction schemes with a large basis set calculation. We start this comparison by calculating potential energy curves for two simple cubic molecular crystals, namely N_2 and NH_3, with the hybrid functional B3LYP and small (SVP) and large (QZVP[64]) basis set. By starting from the experimental crystal structures, the lattice parameter has been varied in a range of -10% $< a <$ +15 % by fixing the internal coordinates of the molecules at their experimental values. In Figure 2, the gCP corrected potential energy curves are shown. In the case of N_2, the curve obtained with the small basis set shows a minimum not far from the experimental lattice constant of 5.649 Å, while the BB-CP corrected one is purely repulsive. This is expected because of the very weak dispersion dominated intermolecular interactions in solid N_2 and of the well known failure of the B3LYP functional in properly describing van der Waals interactions. The artificial minimum is evidently due to the BSSE as confirmed by the results with the larger QVZP basis set which shows only a very small BSSE. The gCP correction removes most of the BSSE and closely reproduces the BB-CP corrected curve. A closer inspection shows that the gCP approach gives a better agreement with BB-CP at shorter lattice parameters, while it overestimates the correction when the cell is expanded. For ammonia (Figure 1 (b)) similar results are found. However, the gCP corrected lattice energies tend to be underestimated with respect to the BB-CP

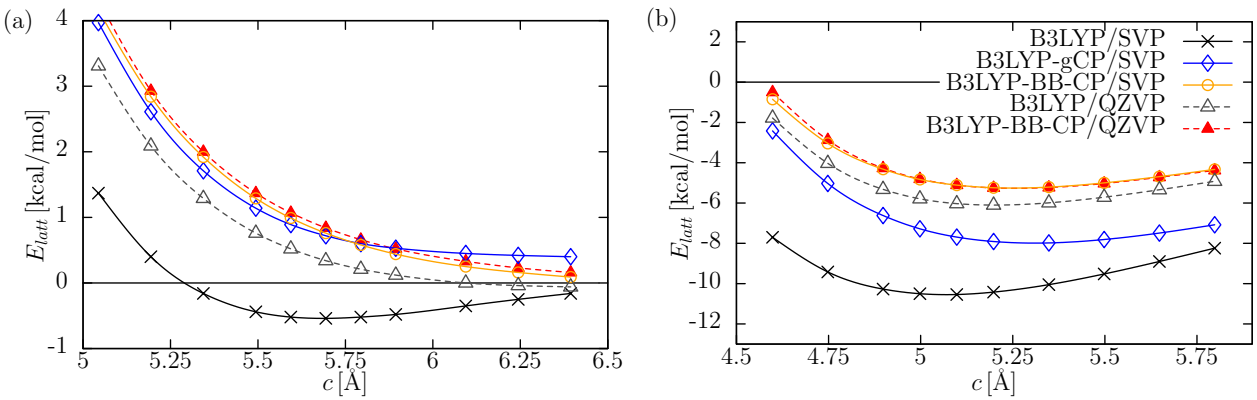

Figure 1: Potential energy curves for (a) N_2 and (b) NH_3 molecular crystals. The lattice parameter is changed around the experimental value. The B3LYP/SVP curves that includes either the gCP and the BB-CP corrections are compared with the B3LYP/QZVP one (with and without BB-CP correction).

ones. Larger deviations are observed as the lattice constant enlarges. Notably, for both molecular crystals, the B3LYP/QZVP results are still affected by some BSSE. This indicates that the utilized QZVP basis still suffers from incompleteness, which leads to a significant BSSE.

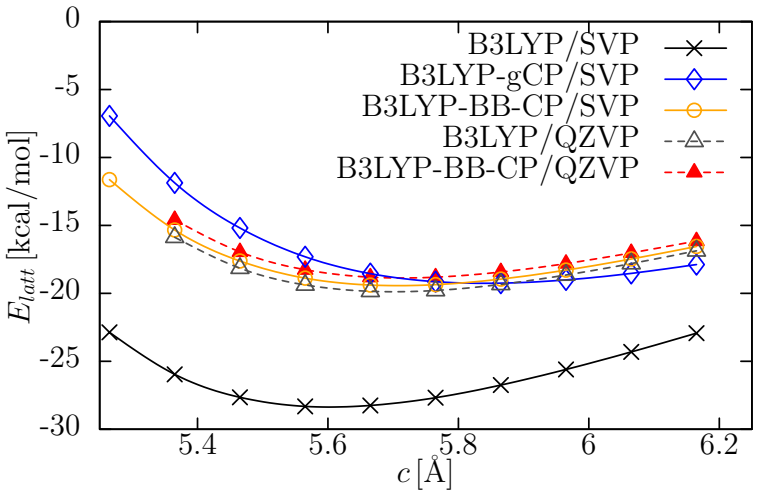

Figure 2: Potential energy curves for urea. The lattice parameter is changed around the experimental value. The B3LYP/SVP curves that includes either the gCP and the BB-CP corrections are compared with the B3LYP/QZVP one (with and without BB-CP correction).

Additionally, we investigate the urea crystal in the same fashion. In order to have a single variable to scan, we adopt the following procedure. By starting from the experimental crystal geometry (tetragonal) as measured at 12 K by neutron powder diffraction[65] the lattice energy is computed as a function of the lattice constant a while the lattice parameter c is varied by fixing the c/a ratio at its experimental value (i.e. 0.8417). We change the lattice parameter in a range between $-5.4\,\%$ and $+10.8\,\%$. Expansion and contraction of the lattice parameters is carried out in a rigid body approach. This means that during the cell deformation the internal geometry of the urea molecule is kept fixed. As can be seen in Figure 2, the crystal is bound on all theoretical levels. This is expected because of the strong hydrogen bonds, which can be properly described by the (semi-)local hybrid functional B3LYP. However, the binding energy is strongly overestimated by 42 % on the B3LYP/SVP level compared to the B3LYP/QZVP result. We correct the small basis calculation with the standard BB-CP correction and with the new gCP scheme. Deviations of the binding energy compared the the B3LYP/QZVP level diminishes to 2 % and 3 % on the B3LYP-

BB-CP/SVP and B3LYP-gCP/SVP levels, respectively. As shown in Figure 2, the gCP curve is in good agreement with the BB-CP and the large QZVP basis set. While the gCP corected energy is very close to the BB-CP corrected one, the minimum is slighly shifted to larger values. This will change the equilibrium in unconstrained geometry optimizations towards too large unit cells. We present a more detailed analysis and work-around in the following section.

Overall, in the three cases, the gCP approach appears to reasonably reproduce the BB-CP correction at least regarding the lattice energies. The shape of the potential energy profile is qualitatively corrected in the right direction but we note a slight inconsistency between crystal energy and geometry. This is important for geometry optimization as will be discussed in the next section. Note that dispersion corrections have not been applied yet which is mandatory when comparisons to experimental data are made as discussed in the next section.

X23 Benchmark Set

A benchmark set for non-covalent interactions in solids consisting of 21 molecular crystals (dubbed C21) was compiled by Johnson[21] recently. Two data sets are considered: (1) thermodynamically

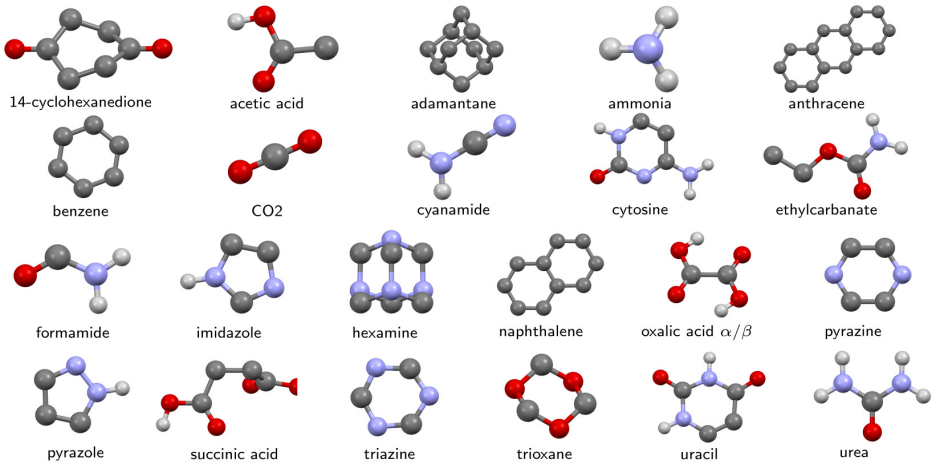

Figure 3: Geometries of the 23 small organic molecules from the X23 benchmark set for non-covalent interactions in solids. H-atoms at carbons are omitted for clarity. Carbons are denoted by dark gray balls, hydrogens are light gray, oxygens are red, and nitrogens are light blue (color online).

Table 1: Mean absolute deviation (MAD), mean deviation (MD), and standard deviation (SD) of the sublimation energy for the X23 test set and for the subset X12/Hydrogen dominated by hydrogen bonds. We calculate the energy with different combinations of functionals (PBE and B3LYP), dispersion correction D3, and geometric counterpoise correction gCP and compare with thermodynamically back-corrected experimental sublimation energies. On the PBE/SVP level, we give values based on deviations to the corresponding large plane-wave basis set values in the SI. All values are in kcal/mol.

	X23			X12/Hydrogen	
Method	MAD	MD	SD	MAD	MD
PBE/CBS	11.7	−11.7	6.1	9.7	−9.7
PBE-D3/CBS	1.1	0.4	1.3	1.3	0.8
PBE-D3/CBS+$E^{(3)a}$	1.2	−0.5	1.7	1.1	0.1
PBE/SVP	5.4	−3.8	7.0	2.6	−0.1
PBE-D3/SVP	8.5	8.5	3.5	10.5	10.5
PBE-D3-gCP/SVP	2.5	−1.1	3.0	2.8	−1.4
PBE-D3-gCP/SVP+$E^{(3)a}$	2.9	−2.0	3.2	3.1	−2.2
B3LYP-D3/SVP	10.1	10.1	4.1	12.0	12.0
B3LYP-D3-gCP/SVP	2.0	0.6	2.2	1.7	−0.1
B3LYP-D3-gCP/SVP+$E^{(3)a}$	1.7	−0.3	2.2	1.8	−0.8

[a] Three-body dispersion single-point energy $E^{(3)}$ on optimized structures.

back-corrected experimental sublimation energies and (2) structural data from low-temperature X-ray diffraction. The thermal and zero-point effects were explicitly accounted for. Therefore, we can directly compare the electronic energy differences with the back-corrected experimental values. The error bar of experimental sublimation energies was estimated to be 1.2 kcal/mol.[66] Recently, the C21 set was extended and refined by Tkatchenko *et. al.*[22] The X23 benchmark set (16 systems are presented in Ref.[22] and seven additional systems were obtained as a private communication from the authors) includes two additional molecular crystals, namely hexamine and succinic acid. The molecular geometries of the X23 set are shown in Figure 3. The details of the back-correction procedure are summarized in Ref.[22] The mean absolute deviation (MAD) between both reference data sets is 0.55 kcal/mol. Because the X23 data seem to be more consistent we use it here as reference. If we take the standard deviation (SD) between both thermodynamic corrections as independent error source, we can add the squared errors to the total uncertainty of the reference

values and obtain about 1.3 kcal/mol as statistical error. We calculate sublimation energies and crystal geometries utilizing the GGA functional PBE and the hybrid GGA functional B3LYP with a small polarized split-valence basis set SVP. The PBE/CBS values are computed with the VASP program package. In the sublimation energy calculations the isolated molecules are approximated by a large unit cell calculation with a minimum distance between molecule images of 16 Å. In

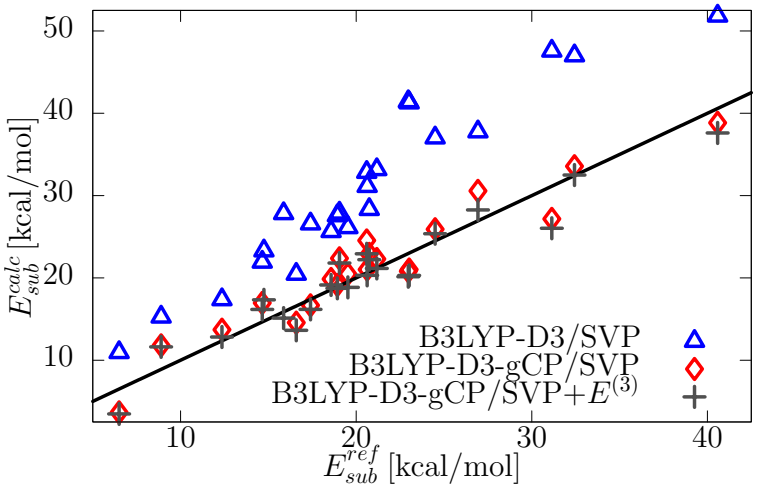

Figure 4: Sublimation energy per molecule for the X23 set on the B3LYP-D3/SVP, B3LYP-D3-gCP/SVP, and B3LYP-D3-gCP/SVP+$E^{(3)}$ levels. We compare with thermodynamically back-corrected experimental energies E_{sub}^{ref}.

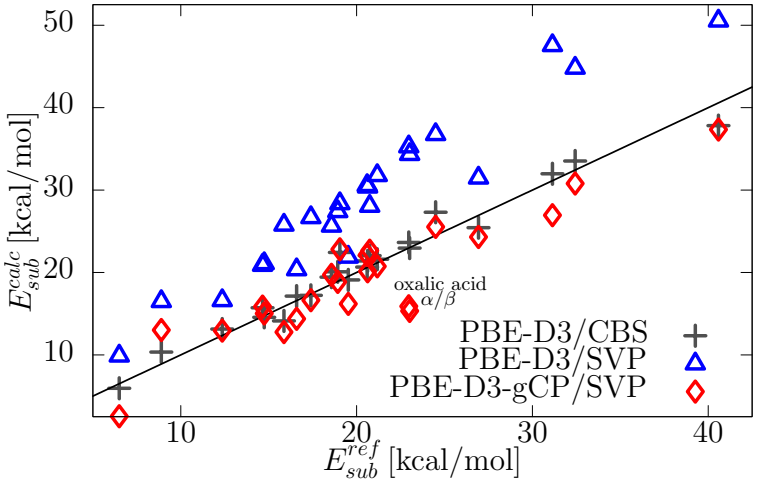

Figure 5: Sublimation energy per molecule for the X23 set on the PBE-D3/SVP and PBE-D3-gCP/SVP levels. We compare with thermodynamically back-corrected experimental energies. The energies are calculated on optimized structures with experimental lattice constants.

order to calculate the sublimation energy, we optimize the isolated molecule and the corresponding

molecular crystal. The unit cells are kept fixed at the experimental values. We summarize the deviations from reference data in Table Table 1. The individual values for all systems are given in the SI. First, the exceptionally small MAD of 1.1 kcal/mol on the PBE-D3/CBS level should be mentioned which is within the estimated experimental error. The importance of the D3 correction is obvious from the huge error of plain PBE/CBS which very strongly underbinds most of the crystals. The D3 uncorrected functional (PBE/SVP) yields a smaller error than the corresponding CBS result which is due to the BSSE. Because of the very encouraging results of the D3 scheme in the estimated CBS limit and the physical significance of dispersion in periodic systems, we will only report and discuss D3 corrected results in the following.

Without BSSE correction, the MADs are 8.5 kcal/mol and 10.1 kcal/mol on the PBE-D3/SVP and B3LYP-D3/SVP level, respectively. The mean deviation (MD) and the MAD are identical meaning that the sublimation energy is artificially overestimated in all tested systems. Utilizing the gCP potential for BSSE correction, the MAD drops drastically to 2.5 kcal/mol and 2.0 kcal/mol, respectively, for the two methods. The BSSE corrected small basis set PBE-D3 results nicely match those at the estimated CBS limit obtained with the BSSE-free plane wave basis. Figure 5 shows the correlation between the PBE-D3(-gCP)/SVP energies and the experimental reference values. The remaining BSE is of the same order of magnitude than the error of the corresponding CBS calculation. Additionally we investigate the effect of three-body dispersion for all levels of theory. The correlation plot between the B3LYP-D3(-gCP)/SVP($+E^{(3)}$) energies and the reference values is shown in Figure 4. The three-body term is repulsive for all systems and significantly improves the results for the B3LYP functional (see Table Table 1). However, the PBE-D3 errors are slightly larger with three-body term. The MAD is 1.7 kcal/mol and 1.2 kcal/mol, respectively, on the B3LYP-D3-gCP/SVP$+E^{(3)}$ and PBE-D3/CBS$+E^{(3)}$ level. Tentatively this can be attributed to the very different many-body behavior of the two functionals for overlapping densities as noted already some years ago.[67]

We compute the deviations separately for hydrogen and non-hydrogen bonded systems to investigate the different energetic contributions. Results are also reported in Table Table 1. On

the PBE-D3/CBS level, the sublimation energies of hydrogen bonded systems (X12/Hydrogen subset) are systematically too large. The systematic overbinding of PBE for such systems is well-known from molecular complexes[32,68] and not unexpectedly transfers to molecular crystals. However, for the small SVP basis the sublimation energies of the X12/hydrogen set are systematically underestimated by 2.2 kcal/mol and by 0.8 kcal/mol on the PBE-D3-gCP/SVP+$E^{(3)}$ and B3LYP-D3-gCP/SVP+$E^{(3)}$ level, respectively. We explain this underbinding by the lack of a second set of polarization functions with smaller exponents. This prevents the system from a proper polarization in an electric field, which is significant in hydrogen bonds. The effect is very dominant in both oxalic acid polymorphs and in succinic acid and explains their larger error (visible in Figure 4 and Figure 5). For both functionals, α/β-oxalic acid have the largest deviation from the reference values. For α-oxalic acid the sublimation energy is overestimated with PBE-D3/CBS by 4.7 kcal/mol, while it is underestimated with PBE-D3-gCP/SVP+$E^{(3)}$ and B3LYP-D3-gCP/SVP+$E^{(3)}$ by 8.4 kcal/mol and 2.7 kcal/mol, respectively. The errors in describing hydrogen bonds with the PBE functional are significantly larger than with the hybrid functional B3LYP.

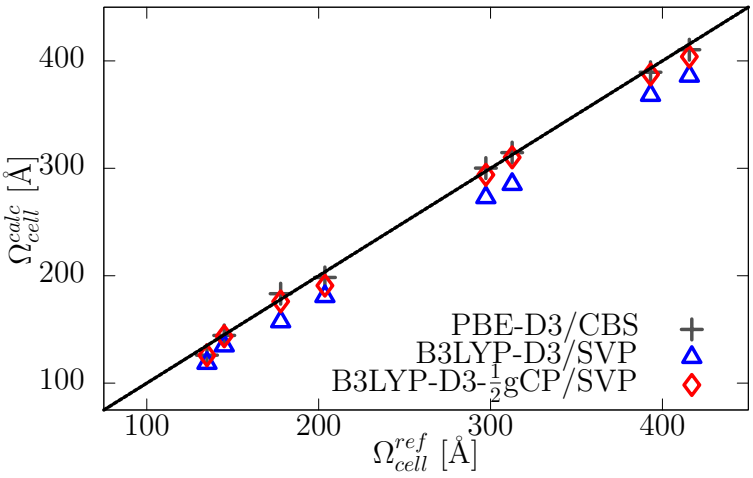

Figure 6: Unit cell volumes for eight representative crystals of the X23 set on the B3LYP-D3/SVP and B3LYP-D3-$\frac{1}{2}$gCP/SVP levels. We compare with experimental low-temperature X-ray data.

For eleven crystals of the X23 set, we perform a full geometry optimization and explore the PBE functional. For eight systems, we additionally investigate the performance of the hybrid functional B3LYP. A more detailed analysis of these structural data is presented in the SI. As most

sensitive observable, we compare the unit cell volume with the experimental values in Table Table 2. Due to thermal length expansions, the calculated zero Kelvin cell volumes should be smaller than the measured ones. Thermal expansions of these systems are estimated to be approximately 3 %, while also larger thermal expansion up to 8 % were reported.[69] The estimated PBE-D3/CBS

Table 2: Mean absolute deviations (MAD) and mean deviation (MD) of the unit cell volumes. We calculate the geometries with different combinations of functionals PBE and B3LYP with SVP basis, dispersion correction D3, and geometric counterpoise correction gCP. Deviations with respect to the CBS values are given in parentheses. Absolute values are in Å^3.

Method	MAD	MD	Rel. MD
PBE-D3/CBS	4.2 (0.0)	−1.5 (0.0)	−0.8%
PBE-D3	17.5 (15.9)	−17.5 (−15.9)	−6.1%
PBE-D3-$\frac{1}{2}$gCP	7.5 (5.8)	−3.3 (4.9)	1.0%
PBE-D3-gCP	23.7 (25.3)	23.7 (25.3)	7.9%
B3LYP-D3	22.1	−22.1	−9.1%
B3LYP-D3-$\frac{1}{2}$gCP	6.6	−6.6	−2.9%

results have a small MAD of 4 Å^3. As expected, the unit cells are systematically too small by 0.8 %. With the SVP basis set, the BSSE artificially shrinks the crystal by on average 6 % on the PBE-D3/SVP level. With the full counterpoise correction we obtain unit cell volumes by 8 % too large. The full BB-CP is known to overestimate the BSSE in large and dense systems.[70] While this seems not to be the case for the sublimation energies, we notice a significant effect on the crystal geometry which, however, at present is not entirely clear. Empirically it has been found before[70–75] that half of the counterpoise correction is a reasonably work around. Indeed, when the gCP correction is reduced to 50 %, a good agreement with the experimental data is obtained. The MAD drops from 17 Å^3 to 7 Å^3 on the PBE-D3/SVP and PBE-D3-$\frac{1}{2}$gCP/SVP levels, respectively. The MADs with respect to the corresponding PBE-D3/CBS values are smaller. This indicates that some of the remaining errors do not arise because of BSE, but rather due to shortcomings of the PBE functional as noted in the previous paragraph. The unit cell volume of the systems dominated by hydrogen bonds has an MD of 5 Å^3 with respect to the CBS estimate, while the non-hydrogen bonded systems have a significantly smaller MD of 2 Å^3. Again, in the description of hydrogen

bonds, B3LYP performs better than PBE. In Figure 6, we show the correlation with the experimental unit cell volumes. Utilizing BSSE uncorrected B3LYP-D3/SVP, the unit cell volumes are underestimated by 9 % while with 50 % of the gCP correction very reasonable geometries, too small by only 3 %, are obtained.

Graphite: Interlayer Distance and Energy

In order to demonstrate the applicability of the gCP correction for denser systems, we investigate the interactions between graphite layers. The experimental interlayer equilibrium distance is 3.34 ± 0.03 Å.[76] The experimental exfoliation energies have a large spread and range from -35 meV to -52 meV per atom.[77–80] We studied a similar system previously and demonstrated the applicability of the semi-empirical dispersion correction DFT-D2.[81,82] The earlier study was done by an extrapolation of different finite size graphene layers. Significant errors were noted utilizing basis sets below the quadruple-ζ level.

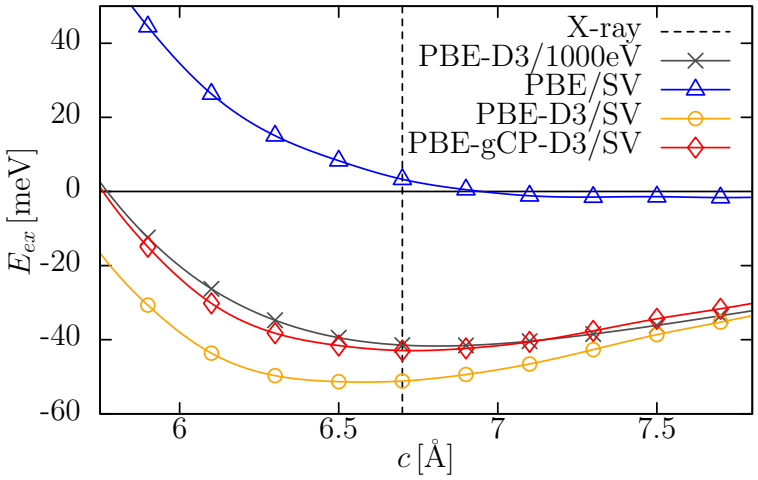

Figure 7: Exfoliation energy E_{ex} of two graphite layers per atom as a function of the stacking distance c. We explore the PBE functional with SV basis and huge PAW (dubbed as CBS) basis sets. The vertical line denotes the experimental value. The cell parameters a and b are fixed to the experimental values.

Here, we describe the system periodically and investigate the effect of BSSE. For our calculations, we use the PBE functional with unpolarized split valence basis set SV. We compute the

interlayer binding energy of graphite for different interlayer distances c (PES) shown in Figure 7. The plain PBE functional shows no significant minimum in the potential energy curve and no net bonding is observed. Adding the D3 correction, the minimum distance is underestimated by 0.2 Å due to BSSE. At the gCP corrected level a perfect agreement between theory and experiment is found. Calculations with huge, BSSE free plane-wave basis sets confirm the identified PBE-D3 minimum. Especially in the minimum region, the agreement between the PBE-D3-gCP/SVP and PBE-D3/CBS results is excellent. We calculate an exfoliation energy of -43.0 meV/atom on the PBE-D3-gCP/SVP level. This is reasonable in comparison to the experimental estimates, and it differs by only 3 % from three PBE-D3/CBS value.

We investigate the same system on the PBE/pob-TZVP level. The additional basis functions increase the BSSE significantly resulting in an artificial minimum at an interlayer distance of 3.2 Å. This seemingly good result arises from an accidental error cancellation. The BSSE gives an artificial attraction which simulates, near the minimum, the neglected dispersion attraction. However, the exponentially decaying BSSE can not accurately mimic the dispersion interaction, which decays as r^{-6} with the interatomic distance for each atom pair. This is demonstrated in Figure 8, where we analyze the long-range behavior of the interlayer interaction on the PBE-D3-gCP/SV and PBE(-D3-gCP)/pob-TZVP levels. We fit a power law $E_{ex} \propto c^{-n}$ in a least-square sense for distances c in the interval $[10, 20]$ Å.

The combination of PBE/SV, D3, and gCP shows the correct asymptotic behavior of c^{-4} for insulating infinite layers. For the special case of graphite (k-point conductor) the true dependence is $c^{-3}\ln(c/c_0)$.[83] We find a critical exponent of 4.03 which nicely agrees with the value of 4.2 as predicted by means of quantum Monte Carlo calculations.[84] On the other hand, the raw PBE functional with a triple-ζ basis exhibits a more exponential behavior (the exponent for the power-law fit is about 18) as expected.

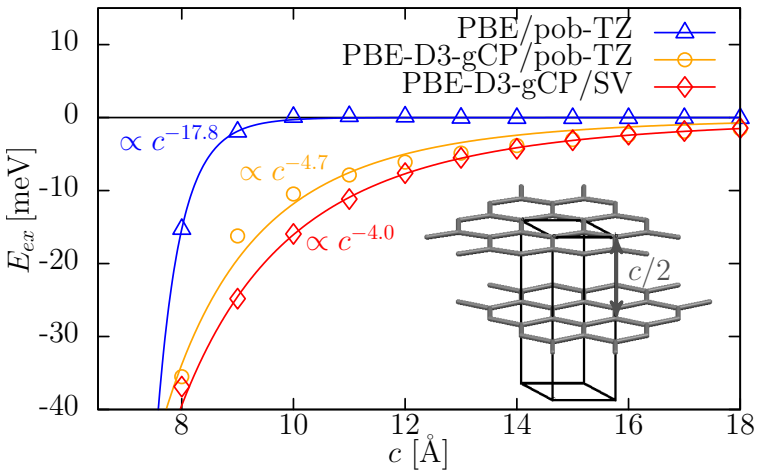

Figure 8: Exfoliation energy E_{ex} of two graphite layers per atom as a function of the stacking distance c in the long-range limit. The continuous lines correspond to a power law fit with critical exponents of 18 and 4 for the PBE/pob-TZVP and PBE-D3-gCP/SV levels, respectively. The cell parameters a and b are fixed to the experimental values.

The gCP correction for the pob-TZVP Basis

We mentioned the problem of near linear dependencies that arises if basis functions with small exponents are included in periodic calculations of dense systems. Even with the Ahlrichs SVP basis set, we encounter some SCF convergence problems. Recently, a new Gaussian basis set, denoted as pob-TZVP, was developed[26] which provided stable and robust SCF convergence for a wide range of solids. However, we demonstrated above, that its BSSE can be huge. The main target of these basis sets are bulk systems or surfaces where both, dispersion interactions and BSSE artifacts are important. Therefore, we determined the gCP parameters for the pob-TZVP basis in the same way as described in the original Ref[18] using the TURBOMOLE program suite.[85] We calculate the e^{miss} parameters for all elements H-Br (excluding rare gases) between the restricted open shell HF energy E_{ROHF} for the target basis and a large quadruple-ζ basis def2-QZVPD according to

$$e^{\text{miss}} = E_{ROHF}^{\text{target basis}} - E_{ROHF}^{\text{large basis}}|_{F=0.06\,au}, \tag{9}$$

where $F = 0.06$ au denotes an applied weak electric field in order to populate higher angular momentum functions. These values can be used to judge the completeness of an atomic basis set

as discussed in the orginal gCP work. In this regard, the pob-TZVP and the SVP basis sets are rather similar, with mean e^{miss} parameters of 0.24 and 0.22 Hartree, respectively. We fit the four parameters σ, α, β, and η in equation Eq. (8) to computed BB-CP data at the B3LYP/pob-TZVP level for the S66x8[44] benchmark set. The optimized parameters are

$$\begin{aligned} \sigma &= 0.1300 & \alpha &= 1.3743 \\ \beta &= 0.4792 & \eta &= 1.3962\,. \end{aligned} \tag{10}$$

The root mean square deviation (RMSD) of the fit for the pob-TZVP and SVP basis sets are 0.002 and 0.001 Hartree, respectively, i.e., the Ahlrichs basis set SVP seems to be better balanced.

For the X23 benchmark set, presented previously, the MAD of the sublimation energies is significantly reduced from 10.7 kcal/mol on the PBE-D3/pob-TZVP level to 4.7 kcal/mol on the PBE-D3-gCP/pob-TZVP level. The asymptotic behavior of the interlayer interation in graphite is also improved. The scaling exponent of 4.72 on the PBE-D3-gCP/pob-TZVP level represents a huge improvement compared to the unphysical value of 17.83 for plain PBE/pob-TZVP. Although the dispersion and BSSE corrected pob-TZVP basis set works reasonably well, we recommend to use the Ahlrichs type basis set for calculations on molecular crystals.

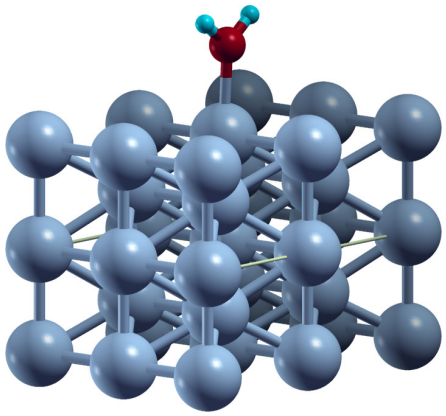

Figure 9: Model system for the adsorption of H_2O on the Ni (110) surface.

One of the most important applications of bulk-optimized basis sets in combination with correction schemes for dispersion and BSSE is the description of adsorption of molecules on sur-

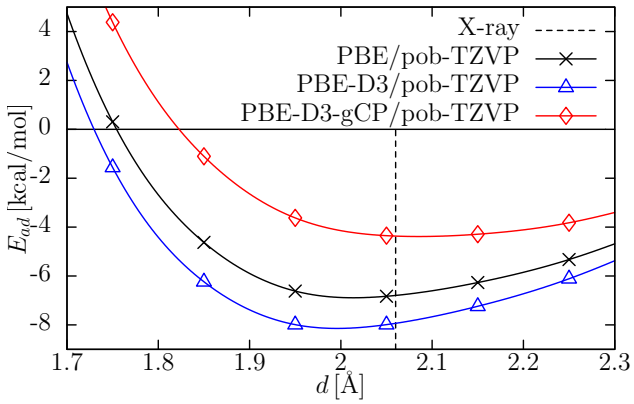

Figure 10: Potential energy surface of the water adsorption on a Ni(110) surface with varying Ni−OH_2 distance d. We utilize the PBE functional with pob-TZVP basis set and explore the effects of D3 and gCP correction, respectively.

faces. Neglecting even one of these effects can lead to significant errors. We therefore demonstrate the application of our periodic BSSE correction scheme for the adsorption of water on Ni (110). Water adsorbs oxygen-down on the Ni (110) surface at a top position. The Ni−OH_2 distance was determined by surface extended X-ray absorption fine structure (SEXAFS) spectroscopy as 2.06 ± 0.03 Å.[86,87]

The Ni bulk was optimized employing the PBE functional and the pob-TZVP basis set. With 3.451 Å for the unmodified pob basis set, the deviation from the experimental lattice constant[88] of 3.524 Å is only 2 %. A 2×2 supercell slab model ($a = 4.881$ Å, $b = 6.902$ Å) with 5 atomic layers was optimized, allowing full relaxation of all atoms. The structure of the water molecule was optimized in the gas phase also employing the PBE functional and the pob-TZVP basis set and set on top of a center Ni atom (see Figure 10).

We varied the Ni−OH_2 bond distance from 1.7 to 2.3 Å, fixing the orientation of the water molecule. Without any correction, PBE/pob-TZVP seems to give the correct value of 2.05 Å. When applying only the D3 correction, a slight overbinding (2.00 Å) is found, while applying only the gCP correction overestimates the bond distance (2.15 Å). Correcting for dispersion as well as for the BSSE, the Ni−OH_2 bond distance (2.05 Å) is in perfect agreement with the experiment.

Conclusions

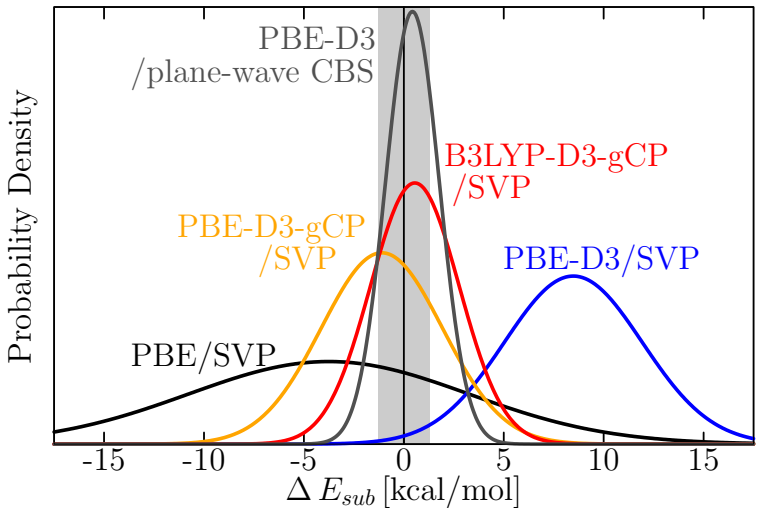

Figure 11: Deviations between experimental sublimation energies of the X23 set and theoretical calculations utilizing the PBE and B3LYP functional and small SVP basis set. The CBS values are estimated with a huge plane-wave basis set with energy cutoff of 1000 eV. The statistical data are converted into normal error distributions. The gray shading denotes the experimental error interval. The quality of the theoretical methods is in the following (declining) order: PBE-D3/CBS, B3LYP-D3-gCP/SVP, PBE-D3-gCP/SVP, PBE-D3/SVP, and PBE/SVP.

We presented and evaluated the semi-empirical geometrical counterpoise correction gCP for usage in periodic DFT calculations. The gCP correction is added to the total (ideally dispersion corrected) DFT energy and approximates the Boys-Bernardi counterpoise energy in a fast and differentiable way for various atom-centered Gaussian basis sets. A benchmark set for non-covalent interactions in solids (X23) is exploited to evaluate the performance of various DFT methods also with small Gaussian AO basis sets. The statistical data for the deviations of computed sublimation energies from reference data are converted to normal error distributions shown in Figure 11. The plane-wave basis set PBE-D3 results are of high quality with an MAD below the estimated experimental uncertainty. From the small basis set calculations, PBE-D3-gCP/SVP and B3LYP-D3-gCP/SVP can also be recommended. The error spread at the PBE/SVP and PBE-D3/SVP levels is significant due to an incomplete account of dispersion and BSSE. This is also true for the B3LYP/SVP calculations if one of the corrections is neglected.

For the computation of the crystal structures at the SVP level, the BSSE seems to be overesti-

mated by the counterpoise corrections. We suggest the following general strategy when small basis sets are employed. First, a geometry optimization using the atom pairwise dispersion correction D3, and 50 % of the gCP correction (dubbed DFT-D3-$\frac{1}{2}$gCP) should be conducted. Subsequently, a single-point energy with two- and three-body dispersion energy and full counterpoise correction on the optimized structure (dubbed DFT-D3-gCP+$E^{(3)}$) should be computed. If hydrogen bonds are present, the B3LYP functional is preferred over PBE. The gCP can be also applied to denser systems as demonstrated by the good results for the graphite stacking on the PBE-D3-gCP/SV level. The interlayer potential agrees remarkably well with BSSE-free, plane-wave results on the PBE-D3/CBS level. The agreement with the experimental interlayer equilibrium interaction energy and distance is satisfactory.

We fitted the gCP parameters for a recently developed solid-state Gaussian basis set (pob-TZVP). For the adsorption of water on a nickel (110) surface as an example, the PBE-D3-gcp/pob-TZVP level was tested. For the Ni-O distance a very good agreement with the experimental value was found.

The gCP method is implemented in a freely available FORTRAN program obtainable from the author's website and will be available in the next release of the CRYSTAL code. Similar to what has been pointed out recently for molecular thermochemistry,[19] it is recommend as a default for dispersion corrected, small basis set DFT or HF calculations also for solids.

Acknowledgement

This work is supported by Deutsche Forschungsgemeinschaft (DFG) under grant SFB813 "Chemistry at Spin Centers - Concepts, Mechanisms, Functions".

Supporting Information Available

Sublimation energies per molecule of all X23 organic crystals. Additional geometry information on the fully optimized structures.

This material is available free of charge via the Internet at `http://pubs.acs.org/`.

References

(1) Sanderson, K. *Nature* **2007**, *450*, 771.

(2) Woodley, S. M.; Catlow, R. *Nature Materials* **2008**, *7*, 937–946.

(3) Neumann, M. A.; Leusen, F. J. J.; Kendrick, J. *Angew. Chem. Int. Ed.* **2008**, *47*, 2427–2430.

(4) Klimes, J.; Michaelides, A. *J. Chem. Phys.* **2012**, *137*, 120901.

(5) Vydrov, O. A.; Van Voorhis, T. *J. Chem. Phys.* **2010**, *133*, 244103.

(6) Civalleri, B.; Zicovich-Wilson, C. M.; Valenzano, L.; Ugliengo, P. *CrystEngComm* **2008**, *10*, 405–410.

(7) Jacobsen, H.; Cavallo, L. *ChemPhysChem* **2012**, *13*, 562–569.

(8) Burns, L. A.; Vazquez-Mayagoitia, A.; Sumpter, B. G.; Sherrill, C. D. *J. Chem. Phys.* **2011**, *134*, 084107.

(9) Nanda, K.; Beran, G. *J. Chem. Phys.* **2012**, *138*, 174106.

(10) Wen, S.; Nanda, K.; Huang, Y.; Beran, G. *Phys. Chem. Chem. Phys.* **2012**, *14*, 7578–7590.

(11) Krukau, A. V.; Vydrov, O. A.; Izmaylov, A. F.; Scuseria, G. E. *J. Chem. Phys.* **2006**, *125*, 224106.

(12) Brandenburg, J. G.; Grimme, S.; Jones, P. G.; Markopoulos, G.; Hopf, H.; Cyranski, M. K.; Kuck, D. *Chem. Eur. J.* DOI: 10.1002/chem.201300761.

(13) Lippert, G.; Hutter, J.; Parrinello, M. *Mol. Phys.* **1997**, *92*, 477–488.

(14) Lippert, G.; Hutter, J.; Parrinello, M. *Theo. Chem. Acc.* **1999**, *103*, 124–140.

(15) Pisani, C.; Dovesi, R.; Roetti, C. *Hartree-Fock Ab Initio Treatment of Crystalline Solids Lecture Notes in Chemistr Series*; Springer Verlag: Berlin, 1988; Vol. 48.

(16) amd B. Civalleri, R. D.; Orlando, R.; Roetti, C.; Saunders, V. *Rev. Comp. Chem.* **2005**, *21*, 21.

(17) Gutowski, M.; Chalasiński, G. *J. Chem. Phys.* **1993**, *98*, 5540.

(18) Kruse, H.; Grimme, S. *J. Chem. Phys.* **2012**, *136*, 154101.

(19) Kruse, H.; Goerigk, L.; Grimme, S. *J. Org. Chem.* **2012**, *77*, 10824–10834.

(20) Grimme, S.; Antony, J.; Ehrlich, S.; Krieg, H. *J. Chem. Phys.* **2010**, *132*, 154104.

(21) de-la Roza, A. O.; Johnson, E. R. *J. Chem. Phys.* **2012**, *137*, 054103.

(22) Reilly, A. M.; Tkatchenko, A. *J. Phys. Chem. Lett.* **2013**, *4*, 1028.

(23) Ferrero, M.; Civalleri, B.; Rerat, M.; Orlando, R.; Dovesi, R. *J. Chem. Phys.* **2009**, *132*, 214704.

(24) Maschio, L.; Usvyat, D.; Schütz, M.; Civalleri, B. *J. Chem. Phys.* **2010**, *132*, 134706.

(25) Maschio, L.; Usvyat, D.; Civalleri, B. *CrystEngComm* **2010**, *12*, 2429–2435.

(26) Peintinger, M. F.; Oliveira, D. V.; Bredow, T. *J. Comput. Chem.* **2013**, *34*, 451–459.

(27) Grimme, S. *WIREs Comput. Mol. Sci.* **2011**, *1*, 211.

(28) Grimme, S.; Ehrlich, S.; Goerigk, L. *J. Comput. Chem.* **2011**, *32*, 1456–1465.

(29) Becke, A. D.; Johnson, E. R. *J. Chem. Phys.* **2005**, *123*, 154101.

(30) Axilrod, B. M.; Teller, E. *J. Chem. Phys.* **1943**, *11*, 299–300.

(31) Casimir, H. B. G.; Polder, D. *Phys. Rev.* **1948**, *73*, 360–372.

(32) Goerigk, L.; Kruse, H.; Grimme, S. *Chem. Phys. Chem* **2011**, *12*, 3421–3433.

(33) Ehrlich, S.; Moellmann, J.; Grimme, S. *Acc. Chem. Res.* **2013**, *46*, 916–926.

(34) Grimme, S. *Chem. Eur. J.* **2012**, *18*, 9955.

(35) Josaa, D.; Rodríguez-Oteroa, J.; Cabaleiro-Lagob, E. M.; neiroa, M. R.-P. *Chem. Phys. Lett.* **2013**, *557*, 170–175.

(36) Chan, B.; Ball, G. E. *J. Chem. Theory Comput.* **2013**, *9*, 2199–2208.

(37) Moellmann, J.; Grimme, S. *Phys. Chem. Chem. Phys.* **2010**, *12*, 8500–8504.

(38) Reckien, W.; Janetzko, F.; Peintinger, M. F.; Bredow, T. *J. Comput. Chem.* **2012**, *33*, 2023–2031.

(39) J. Moellmann, R. T., S. Ehrlich; Grimme, S. *J. Phys.: Condens. Matter* **2012**, *24*, 424206.

(40) J. C. Sancho-García and J. Aragó and E. Ortí and Y. Olivier, *J. Chem. Phys.* **2013**, *138*, 204304.

(41) von Lilienfeld, O. A.; Tkatchenko, A. *J. Chem. Phys.* **2010**, *132*, 234109.

(42) Tkatchenko, A.; DiStasio, R. A.; Car, R.; Scheffler, M. *Phys. Rev. Lett.* **2012**, *108*, 236402.

(43) Boys, S.; Bernardi, F. *Mol. Phys.* **1970**, *19*, 553–566.

(44) Řezáč, J.; Riley, K. E.; Hobza, P. *J. Chem. Theory Comput.* **2011**, *7*, 2427.

(45) Schäfer, A.; Horn, H.; Ahlrichs, R. *J. Chem. Phys.* **1992**, *97*, 2571–2577.

(46) Schäfer, A.; Huber, C.; Ahlrichs, R. *J. Chem. Phys.* **1994**, *100*, 5829–5235.

(47) Weigend, F.; Ahlrichs, R. *Phys. Chem. Chem. Phys.* **2005**, *7*, 3297–305.

(48) Tatewaki, H.; Huzinaga, S. *J. Comput. Chem.* **1980**, *1*, 205–228.

(49) Schuchardt, K. L.; Didier, B. T.; Elsethagen, T.; Sun, L.; Gurumoorthi, V.; Chase, J.; Li, J.; Windus, T. L. *Journal of Chemical Information and Modeling* **2007**, *47*, 1045–1052.

(50) Hehre, W. J.; Ditchfield, R.; Pople, J. A. *J. Chem. Phys.* **1972**, *56*, 2257–2262.

(51) Dovesi, R.; Orlando, R.; Civalleri, B.; Roetti, C.; Saunders, V. R.; Zicovich-Wilson, C. M. *Z. Kristallogr.* **2005**, *220*, 571.

(52) Dovesi, R.; Saunders, V. R.; Roetti, C.; Orlando, R.; Zicovich-Wilson, C. M.; Pascale, F.; Civalleri, B.; Doll, K.; Harrison, N. M.; Bush, I. J.; D'Arco, P.; Llunell, M. CRYSTAL09 User's Manual (University of Torino, Torino, 2009).

(53) Perdew, J. P.; Burke, K.; Ernzerhof, M. *Phys. Rev. Lett.* **1996**, *77*, 3865–3868.

(54) Perdew, J. P.; Burke, K.; Ernzerhof, M. *Phys. Rev. Lett.* **1997**, *78*, 1396–1396.

(55) Becke, A. D. *J. Chem. Phys.* **1993**, *98*, 5648.

(56) Stephens, P. J.; Devlin, F. J.; Chabalowski, C. F.; Frisch, M. J. *J. Phys. Chem.* **1994**, *98*, 11623.

(57) Monkhorst, H. J.; Pack, J. D. *Phys. Rev. B* **1976**, *13*, 5188–5192.

(58) Kresse, G.; Furthmüller, J. *Comput. Mat. Sci.* **1996**, *6*, 15–50.

(59) Bucko, T.; Hafner, J.; Lebegue, S.; Angyan, J. G. *J. Phys. Chem. A* **2010**, *114*, 11814–11824.

(60) Blöchl, P. E. *Phys. Rev. B* **1994**, *50*, 17953–17979.

(61) Kresse, G.; Joubert, D. *Phys. Rev. B* **1999**, *59*, 1758–1775.

(62) Grimme, S. ANCOPT: Approximate Normal Coordinate Rational Function Optimization Program, Universität Bonn, 2013.

(63) Eckert, F.; Pulay, P.; Werner, H.-J. *J. Comput. Chem.* **1997**, *18*, 1473–1483.

(64) Thakkar, A. J.; Koga, T.; Saito, M.; Hoffmeyer, R. E. *Int. J. Quantum Chem. Symp.* **1993**, *48*, 343.

(65) Swaminathan, S.; Craven, B. M.; McMullan, R. K. *Acta Crystallogr. Sec. B* **1984**, *40*, 300–306.

(66) Chickos, J. S. *Netsu Sokutei* **2003**, *30*, 116.

(67) Tkatchenko, A.; von Lilienfeld, O. A. *Phys. Rev. B* **2008**, *78*, 045116.

(68) Goerigk, L.; Grimme, S. *Phys. Chem. Chem. Phys.* **2011**, *13*, 6670–6688.

(69) Boese, R.; Weiß, H.-C.; Bläser, D. *Angew. Chem.* **1999**, *111*, 1042–1045.

(70) Risthaus, T.; Grimme, S. *J. Chem. Theory Comput.* **2013**, *9*, 1580–1591.

(71) Hyla-Kryspin, I.; Haufe, G.; Grimme, S. *Chem. Eur. J.* **2004**, *10*, 3411–3422.

(72) Karton, A.; Tarnopolsky, A.; Lamère, J.-F.; Schatz, G. C.; Martin, J. M. L. *J. Phys. Chem. A* **2008**, *112*, 12868–12886.

(73) Zhao, Y.; Truhlar, D. G. *Phys. Chem. Chem. Phys.* **2008**, *10*, 2813–2818.

(74) Zhao, Y.; Schultz, N. E.; Truhlar, D. G. *J. Chem. Theory Comput.* **2006**, *2*, 364–382.

(75) Kim, K. S.; Tarakeshwar, P.; Lee, J. Y. *Chem. Rev.* **2000**, *100*, 4145–4186.

(76) Wu, J.; Pisula, W.; Müllen, K. *Chem. Rev.* **2007**, *107*, 718–747.

(77) Girifalco, L. A.; Lad, R. A. *J. Chem. Phys.* **1956**, *25*, 693–698.

(78) Trickey, S. B.; Müller-Plathe, F.; Diercksen, G. H. F. *Phys. Rev. B* **1992**, *45*, 4460–4468.

(79) Benedict, L. X.; .Chopra, N. G.; Cohen, M. L.; Zettl, A.; Louie, S. G.; Crespi, V. H. *Chem. Phys. Lett.* **1998**, *286*, 490–496.

(80) Zacharia, R.; Ulbricht, H.; Hertel, T. *Phys. Rev. B* **2004**, *69*, 155406–155413.

(81) Grimme, S.; Mück-Lichtenfeld, C.; Antony, J. *J. Phys. Chem. C* **2007**, *111*, 11199.

(82) Grimme, S. *J. Comput. Chem.* **2006**, *27*, 1787–1799.

(83) Dobson, J. F.; White, A.; Rubio, A. *Phys. Rev. Lett.* **2006**, *96*, 073201.

(84) Spanu, L.; Sorella, S.; Galli, G. *Phys. Rev. Lett.* **2009**, *103*, 196401.

(85) TURBOMOLE 6.4: R. Ahlrichs, M. K. Armbruster, M. Bär, H.–P. Baron, R. Bauernschmitt, N. Crawford, P. Deglmann, M. Ehrig, K. Eichkorn, S. Elliott, F. Furche, F. Haase, M. Häser, C. Hättig, A. Hellweg, H. Horn, C. Huber, U. Huniar, M. Kattannek, C. Kölmel, M. Kollwitz, K. May, P. Nava, C. Ochsenfeld, H. Öhm, H. Patzelt, D. Rappoport, O. Rubner, A. Schäfer, U. Schneider, M. Sierka, O. Treutler, B. Unterreiner, M. von Arnim, F. Weigend, P. Weis and H. Weiss. Universität Karlsruhe 2012. See also: http://www.turbomole.com.

(86) Henderson, M. A. *Surface Science Reports* **2002**, *46*, 1–308.

(87) Pangher, N.; Schmalz, A.; Haase, J. *Chem. Phys. Lett.* **1994**, *221*, 189–193.

(88) Chichagov, A. V.; Varlamov, D. A.; Dilanyan, R. A.; Dokina, T. N.; Drozhzhina, N. A.; Samokhvalova, O. L.; Ushakovskaya, T. V. *Crystallography Reports* **2001**, *46*, 876–879.

Graphical TOC Entry